ROYAL SOCIETY
OF CHEMISTRY

PAPER

Check for updates

Preparation of a biochar-lignosulfonate composite material and its adsorption performance for Cu²⁺†

Ying Zhang, [ID] ‡*[ab] Qi He,‡[ab] Yonglin Yang[c] and Qian Bai[d]

Biochar was prepared using peanut shells as raw materials, and then composite amino-functionalized lignosulfonate was used to prepare a biochar/lignosulfonate adsorbent (BC-CLS). The morphology and structure of BC-CLS were characterized using FT-IR, SEM, zeta potential, and XPS. The adsorption performance of BC-CLS was evaluated by batch adsorption experiments and dynamic adsorption experiments (adsorption column flow adsorption). The results showed that BC-CLS adsorbent exhibited significant adsorption performance for Cu²⁺, including a short equilibrium time (50 min), fast adsorption rate (11 mg g⁻¹ min⁻¹), and high static saturation adsorption capacity (354 mg g⁻¹). Dynamic adsorption experiments indicated that the maximum adsorption capacity of BC-CLS adsorbent was approximately 280 mg g⁻¹, with a removal rate of over 99% after five cycles, meeting the wastewater discharge standard (less than 1 mg L⁻¹). The results demonstrated that the adsorption capacity of BC-CLS adsorbent for Cu²⁺ was controlled by multiple adsorption mechanisms, including electrostatic attraction, precipitation, and metal ion complexation. Additionally, under pH = 5 conditions, using a 40 mg per L Cu²⁺ solution, the adsorption performance of BC-CLS adsorbent remained above 60% after five adsorption–desorption experiments, indicating good cycling stability of BC-CLS adsorbent.

1 Introduction

Heavy metal ion pollution has always been a major challenge to environmental governance as heavy metal ions can cause serious ecological damage. Heavy metal ions in the environment can affect plant growth, cannot be biodegraded, and can accumulate in organisms, ultimately transferring to higher-level organisms through the food chain, posing a threat to the entire biosphere.[1–3] There are various types of pollutants in wastewater, with copper ion pollution being the most common. Wastewater from electroplating and metal processing industries contains high levels of copper, ranging from tens to hundreds of milligrams per liter. Irrigation of farmland with copper-containing wastewater can lead to copper accumulation in the soil and crops, resulting in poor crop growth, especially in rice and barley, and contamination of grain. The critical concentration of copper sulfate in irrigation water for rice is

0.6 mg L⁻¹. Researchers around the world have been developing new treatment methods and materials to reduce these pollutants. Some of these methods have been widely used to remove heavy metal ions, including biological treatment, filtration, oxidation, and adsorption.[4–7]

Adsorption is a physical and chemical method described as a simple and economically viable wastewater treatment method.[8,9] In this process, the pore structure and chemical surface of the adsorbent material play an important role in selectively removing specific ions from the solution.[10–12] Activated carbon is one of the most widely used adsorbent materials for removing organic and inorganic pollutants in the adsorption process. Due to their adsorption performance and high surface area, they can be used for purification, detoxification, deodorization, and filtration processes. These applications have received attention in various fields, especially in the treatment of drinking water, industrial wastewater, and air.[13–15] However, the high cost of commercial activated carbon has prompted people to seek new, abundant, and inexpensive precursors primarily derived from renewable resources for large-scale use.[16–20]

Peanuts are a common crop, with a peanut production of 18 million tons in China in 2022, resulting in 5 million tons of peanut shells. Peanut shells contain more than 40% carbon, making them suitable for the production of biochar.[21] Peanut shells contain polyphenols such as catechol, pyrogallic acid, and phloroglucinol, and the hydrogen atoms in the phenolic hydroxyl groups can easily exchange with heavy metal ions. Therefore, peanut shells are an ideal choice as adsorbents for heavy metal

ᵃDepartment of Chemical Power Engineering, Shenmu Vocational & Technical College, Yulin 719300, Shaanxi, China. E-mail: zhangying312@163.com

ᵇProduction and Operation Department, Shenmu Electrochemical Development Co., Ltd, Yulin 719300, Shaanxi, China

ᶜSchool of Chemistry & Chemical Engineering, Yulin University, Yulin 719000, Shaanxi, China

ᵈSchool of Mechanical Engineering, Yulin Vocational & Technical College, Yulin 719000, Shaanxi, China

† Electronic supplementary information (ESI) available. See DOI: https://doi.org/10.1039/d4ra00588k

‡ Ying Zhang and Qi He contributed equally to this work.

ions in wastewater treatment.[22–25] In rural areas, locals use peanut shells to plug sewage outlets for clean water. Lignin is an amorphous polymer formed by connecting phenylpropane units through carbon–carbon and ether bonds, and it is the second largest biomass resource in the plant kingdom after cellulose.[26–28] As a typical biomass material, lignin is one of the few renewable resources in aromatic compounds. In recent years, lignin has also become a popular adsorbent material for heavy metal ions. Xiao et al.[28] used lignin to synthesize lignin-based nanotraps (LBNT) adsorbents, which showed removal rates of >99% for soft ions (Ag(I), Hg(II), Cd(II)) and edge ions (Pb(II), Cu(II), Zn(II)), reducing their residual concentrations from 5 mg L^{-1} to 3–9 μg L^{-1}, below the drinking water limit set by the World Health Organization (WHO). Popovic et al.[29] used sulfated lignin as a raw material and achieved maximum adsorption capacities of 74.84, 54.20, 53.12, and 49.42 mg g^{-1} for Cd^{2+}, Cr(VI), As(V), and Ni^{2+} ions, respectively. Wang et al.[30] combined biological carbon and lignin to form CCLA adsorption material, and its adsorption performance for organic dyes was better than that of biological carbon, indicating that the adsorption performance of biological carbon combined with lignin would be enhanced. Therefore, the treatment of heavy metal ions by the composite material of two substances has great potential.

In this study, biochar was prepared from peanut shells and combined with lignin to form a biochar/lignin adsorbent, which was applied to remove Cu^{2+} from aqueous solutions. This not only allows for the reuse of agricultural waste but also helps to address environmental issues.

2 Material and experiment

2.1 Material

Lignosulfonic acid sodium (biopure), glacial acetic acid (analytical pure), acetaldehyde (analytical pure), glutaraldehyde (analytical pure), anhydrous ethanol (analytical pure), copper nitrate and other reagents were purchased from Shanghai McLin Biochemical Technology Co., Ltd, and other reagents are chemical pure. The deionized water used in the experimental process comes from the laboratory's water purification system.

2.2 Preparation of BC-CLS

Wash, dry, crush, sieve, and take 100 mesh peanut shells and place them in a dryer for later use. Take an appropriate amount of crushed peanut shell debris and pour it into a crucible placed in a muffle furnace. Use an anaerobic method to heat it up to 450 °C for 6 hours, then remove it and let it cool naturally. Soak it in a 1 mol L^{-1} dilute hydrochloric acid solution for 12 hours, filter it, wash it with deionized water until neutral, and dry it to obtain biochar, which is then placed in a dryer for later use.[31,32]

Add 5.0 g of lignin sodium sulfonate to 100 mL of deionized water, and slowly add 5 mL of triethylene tetramine at 60 °C water bath for 120 minutes. Then add 2.0 g of biochar and 10 mL of glutaraldehyde, and heat it at 60 °C water bath for 180 minutes. Filter, wash, and dry to obtain a brown powder (BC-CLS).

2.3 Material characterization

The physicochemical properties of MLS were analyzed by various characterization methods. The surface morphology of MLS was recorded by scanning electron microscopy (SEM, Shimadzu SS 550, USA). The infrared spectrum of MLS were characterized by Fourier transform infrared spectroscopy (FTIR, Antaris II, USA). Thermogravimetric analyzer (TGA, STA 449C, Germany) was used to test the thermal stability of LS and MLS. The surface chemical composition of MLS before and after adsorption was determined by X-ray spectrometer (XPS, Escalab 250Xi, USA). The solution concentration of Cu^{2+} before and after adsorption was measured by flame graphite furnace spectrometer atomic absorption spectrophotometer (Shimadzu spectrometer, AA6800, Japan). The surface charge of BC-CLS was determined using a zeta potential analyser (Zetasizer Pro, Malvern Panalytical, USA). A certain amount of BC-CLS was weighed and added to ultrapure water at a solid–liquid ratio of 0.8 g L^{-1} (consistent with the adsorption experiments), and the pH of the solution was adjusted to 2–11 with 0.1 mol L^{-1} HCl and NaOH, and the solution zeta potential was measured after equilibrium, and the average value was determined for three times at each point. The isoelectric point of BC-CLS (pH$_{pzc}$) was the pH value when the zeta potential was The isoelectric point of BC-CLS (pH$_{pzc}$) is the pH value when the zeta potential is zero.

2.4 Batch adsorption experiments

All static adsorption studies were conducted by continuously stirring 10 mg of BC-CLS adsorbent in 100 mL of Cu^{2+} solution at room temperature for 60 min. The adsorption performance of Cu^{2+} was studied in batch adsorption experiments at different contact times (0–300 min), initial Cu^{2+} concentrations (10–400 mg L^{-1}) and initial pH values (2.0–5.5). To evaluate the adsorption–desorption of BC-CLS adsorbent, hydrochloric acid was used as the eluent (pH = 1) to recover the adsorbed Cu^{2+}, and cyclic experiments were conducted using a 40 mg L^{-1} Cu^{2+} solution at pH = 5.5. In addition, the experimental data were fitted with two adsorption isotherm models (Langmuir and Freundlich models) and two adsorption kinetic models (pseudo-first-order and pseudo-second-order) to further analyze the adsorption behavior of BC-CLS adsorbent towards Cu^{2+}. The dynamic adsorption experiment of Cu^{2+} was conducted using a homemade continuous adsorption apparatus. The remaining Cu^{2+} concentration was estimated by centrifuging the BC-CLS adsorbent and using a flame atomic absorption spectrometer. The adsorption capacity and removal efficiency of BC-CLS adsorbent for Cu^{2+} were calculated using formula (1) and (2).

$$q_m = \frac{(C_0 - C_e)V}{m} \quad (1)$$

$$W = \frac{C_0 - C_m}{C_0} \times 100\% \quad (2)$$

where, C_0 and C_m represent the initial and final concentration of Cu (mg L^{-1}), V represents the volume of the solution (L), and m represents the mass of BC-CLS adsorbent (g).

Pseudo-first order model:

$$q_t = q_e(1 - e^{-k_1 t}) \tag{3}$$

Pseudo-second order model:

$$q_t = \frac{k_2 q_e^2 t}{1 + k_2 q_e t} \tag{4}$$

In these two equations, the adsorption amount of BC-CLS on Cu^{2+} at equilibrium and time t are expressed by q_e (mg g^{-1}) and q_t (mg g^{-1}), respectively. The adsorption rate constants associated with the two kinetic models are k_1, k_2.

Intraparticle diffusion model:

$$q_t = k_p t^{0.5} + C \tag{5}$$

where, q_t (mg g^{-1}) is the adsorption capacity of the adsorbent at time t, t (min) is the adsorption time, k_p (mg g^{-1} min$^{-1/2}$) is the intraparticle diffusion rate constant, and C is the correlation constant of intraparticle diffusion.

Langmuir:

$$q_e = \frac{q_m K_L C_e}{1 + K_L C_e} \tag{6}$$

Freundlich:

$$q_e = K_F C_e^{1/n} \tag{7}$$

Here, the adsorption amount of BC-CLS to Cu^{2+} at equilibrium is expressed by q_e (mg g^{-1}), C_e (mg L^{-1}) represents the residual concentration of pollutants in the solution at the adsorption equilibrium. Besides, K_L is the Langmuir constant related to adsorption energy, n and K_F are both Freundlich constant.

Temkin isotherm model:

$$q_e = B \ln A + B \ln C_e \tag{8}$$

where, B represents the equilibrium constant related to adsorption heat; A (mg L^{-1}) represents the constant related to adsorption capacity.

2.5 Column adsorption experiments

A glass column of 25 mm diameter and 1000 mm length was used, filled with 700 mm of BC-CLS adsorbent, and a certain concentration of Cu^{2+} solution flowed down the top of the column at a flow rate of 2 L h^{-1} through the first column as the first column adsorption cycle. The calculation of the first column adsorption capacity Q_1 is shown in eqn (9).

$$Q_1 = \frac{(C_0 - C_1)V_1}{m} \tag{9}$$

where, C_0 and C_1 represent the initial and post-first cycle solution concentrations of Cu (mg L^{-1}), V_1 represents the volume of solution flowing through the first column (L), and m represents the mass of BC-CLS adsorbent (g).

2.6 Adsorption–desorption experiment

In this study, a 50 mL solution of Cu^{2+} with a concentration of 100 mg g^{-1} was prepared and 0.01 g of BC-CLS (biochar-chloride surfactant complex) was added for adsorption experiments. After allowing the mixture to stand for 120 minutes, the adsorption capacity of BC-CLS, denoted as Q_1, was measured. Subsequently, BC-CLS was separated from the solution through filtration and placed in a 0.1 mol L^{-1} HCl solution for desorption for 120 minutes. Following desorption, BC-CLS was again placed in the same Cu^{2+} solution, and its adsorption capacity, denoted as Q_2, was measured. The ratio of Q_2 to Q_1 was calculated to evaluate the re-adsorption efficiency of BC-CLS.

3   Results and discussion

3.1   MLS characterization

As can be seen from Fig. 1a, BC has a lamellar structure. However, the surface structure of BC-CLS is completely different from that of BC, which presents a porous structure. The combination of lignosulfonate and biochar changed its structure. In addition, as can be seen in Fig. 1b, the structure of BC-CLS has clearly changed compared to biochar, indicating that the substance has been altered. As can be seen from Fig. S1,† the surface area of BC-CLS increased relative to BC.

Fig. 2 shows the infrared spectra of BC, CLS, and BC-CLS. In Fig. 2, it can be seen that the infrared spectrum of BC has few absorption peaks and is similar to graphite. CLS and BC-CLS have similar absorption peaks at many positions, such as the O–H stretching vibration absorption peak near 3400 cm^{-1},[33] the three characteristic absorption peaks of C=C
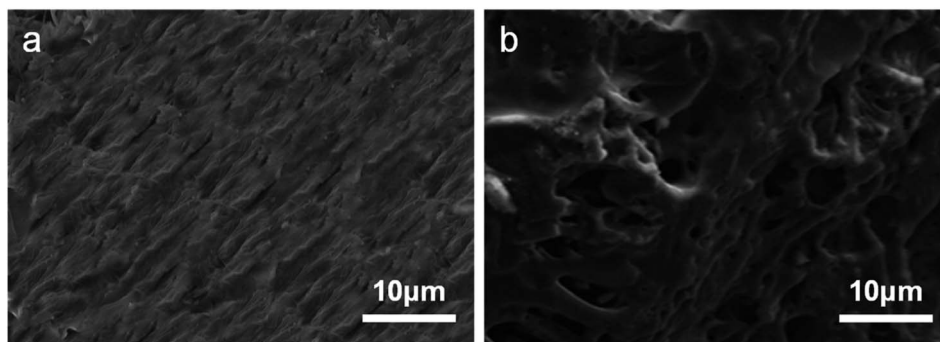

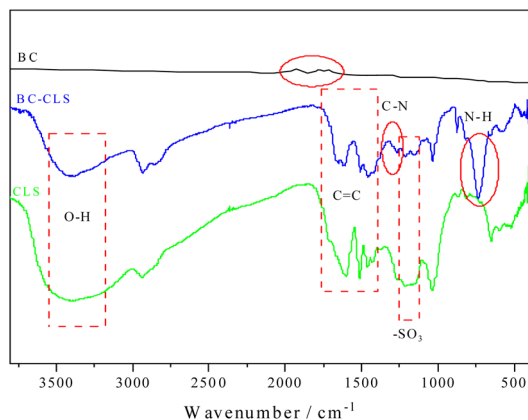Fig. 1   Scanning electron microscopy of BC (a) and BC-CLS (b).

Fig. 2 FT-IR spectra of BC, CLS and BC-CLS.

in the benzene ring near 1600 cm^{-1}, 1500 cm^{-1}, and 1450 cm^{-1},[34] and the characteristic peak of the sulfonic acid group near 1030 cm^{-1}. The presence of multiple identical functional groups indicates the presence of CLS composites on BC-CLS. However, BC-CLS has some unique absorption

peaks, such as the C–N stretching vibration absorption peak at 1260 cm^{-1} (ref. 35) and the N–H vibration absorption peak of alkenes appearing at 870 cm^{-1}.[36] This is the manifestation of triethylenetetramine appearing on BC-CLS, which indicates the successful synthesis of BC-CLS adsorbent.

3.2 Effect of environmental conditions

As shown in Fig. 3a, the influence of pH was studied within the range of pH (2.0–5.5). The adsorption capacity of BC-CLS increased continuously from pH 2.0 to 4.0 and remained constant from pH 4.0 to 5.5. Fig. 3b shows that the pH$_{pzc}$ of BC-CLS is 6.53. When BC-CLS is at pH > pH$_{pzc}$, it carries a negative charge, which is favorable for the electrostatic adsorption of copper ions. However, due to the strong competition from H$^+$, BC-CLS exhibits lower copper ion adsorption capacity at low pH (2.0–3.0). As the pH value increases, the competition from H$^+$ becomes weaker. In addition, the protonation of active sites on the adsorbent surface at low pH values leads to a decrease in the number of active sites binding copper, resulting in low adsorption capacity for copper ions. When the pH increases, the
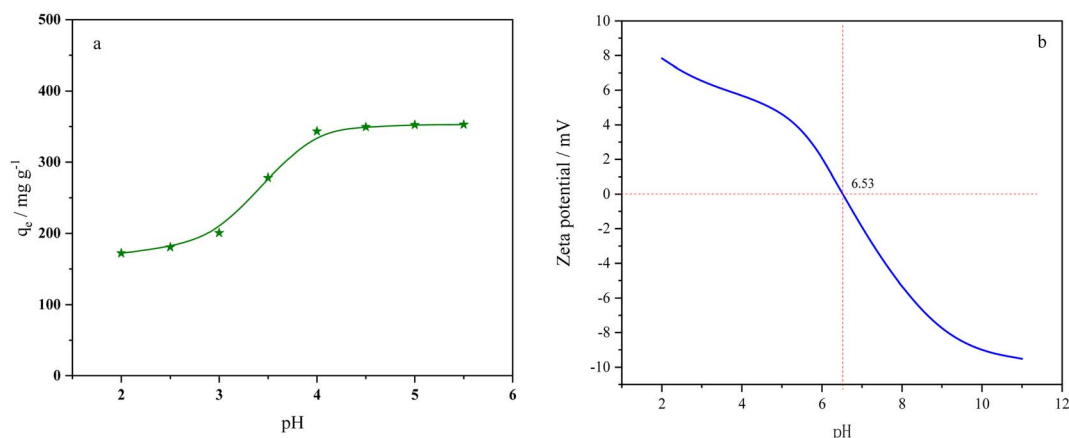

Fig. 3 Effect of solution pH on adsorption capacity of BC-CLS (a) and relationship between zeta potential and pH of BC-CLS (b) (experiment condition: adsorbent dose 0.01 g, temperature 298 K, pH 2–11, time 120 min, concentration 100 mg g^{-1}, solution volume 50 mL).
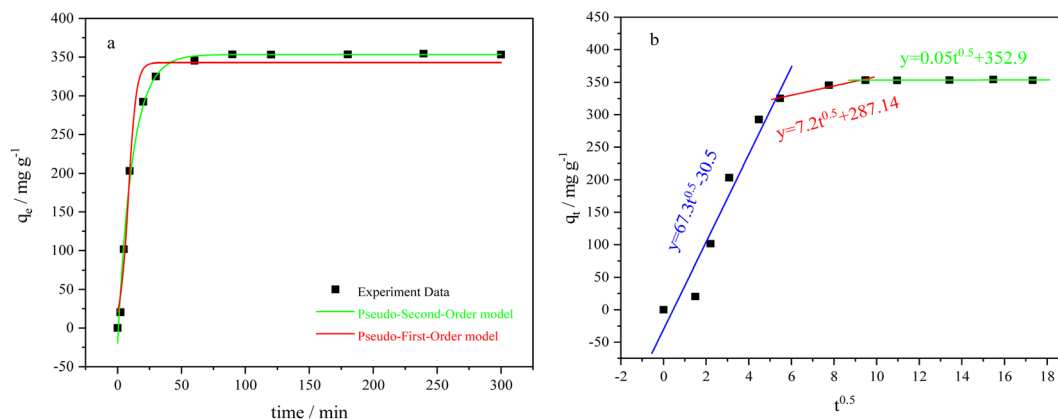

Fig. 4 Adsorption capacity of BC-CLS under different contact times, the corresponding pseudo-first-order, pseudo-second-order kinetics (a) and intra-particle diffusion model (experiment condition: adsorbent dose 0.01 g, temperature 298 K, pH 5, time 5–300 min, concentration 100 mg g^{-1}, solution volume 50 mL).

Table 1 Parameters for the kinetic adsorption data using different adsorption models

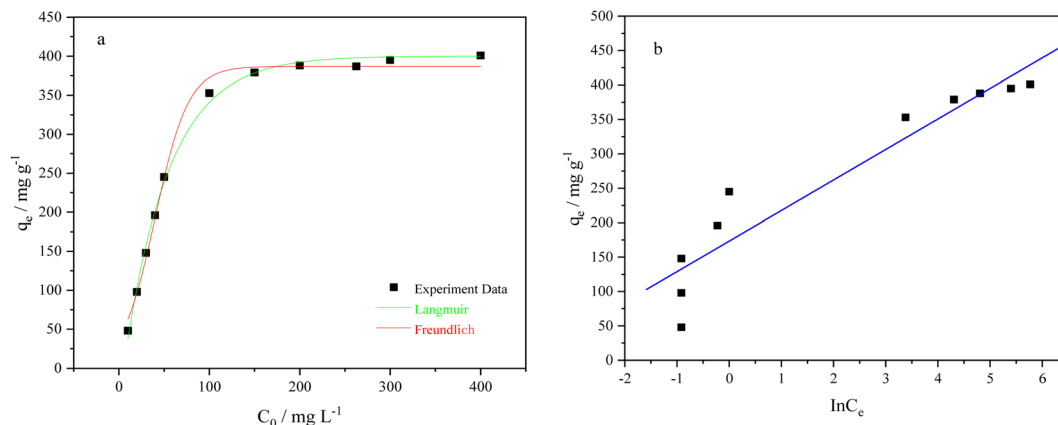| Adsorbate	C_0 (mg g^{-1})	Pseudo-first-order			Pseudo-second-order		
		k_1 (L min^{-1})	$Q_{e,cal}$ (mg g^{-1})	R^2	k_2 (g (mg^{-1} min^{-1}))	$Q_{e,cal}$ (mg g^{-1})	R^2
Cu^{2+}	100	0.027	342.9	0.9659	0.0056	350.8	0.9813

Fig. 5 The adsorption capacity of BC–CLS under different initial concentrations of Cu, the corresponding Langmuir, Freundlich adsorption models (a) and Temkin model (b) (experiment condition: adsorbent dose 0.01 g, temperature 298 K, pH 5, time 120 min, concentration 10–400 mg g^{-1}, solution volume 50 mL).

deprotonation of active sites on BC-CLS is significantly enhanced, making it easier for BC-CLS to capture copper ions.

3.3 Adsorption process

Fig. 4a shows the rapid increase in adsorption capacity of BC-CLS within the first 30 minutes of contact with Cu. This is because there are a large number of adsorption sites on the surface of BC-CLS, and Cu can occupy these adsorption sites quickly, and the adsorption rate at this time can reach 11 mg g^{-1} min^{-1}. Subsequently, the adsorption rate slows down until reaching equilibrium at 50 minutes. This is attributed to a decrease in available adsorption sites and the repulsion between Cu ions already occupying the sites and Cu ions in the solution, which affects the adsorption rate. From Table 1, it can be seen that the pseudo-second-order model shows higher fitting correlation coefficients compared to the pseudo-first-order model, indicating that the adsorption behaviour of BC-CLS is better described by pseudo-second-order kinetics, revealing that BC-CLS adsorbs copper by chemisorption. As the contact time increases, the adsorption rate of Cu on BC-CLS significantly slows down, suggesting that the adsorption time plays an important role in the transfer of Cu from the liquid phase to the adsorbent. Fig. 4b shows that particle diffusion is controlled by three steps. In the initial stage of the first reaction, the adsorption amount increases with the increase of $t^{0.5}$, which is the diffusion stage of metal ions in the boundary layer. With the progress of the reaction, the adsorption capacity of the second stage still increases with the increase of $t^{0.5}$, but the slope decreases and the adsorption rate decreases compared with the previous stage, because the process is controlled by

intra-particle diffusion. As the reaction continues, at the third slow stage, the line flattens out and the adsorption reaches equilibrium (Fig. 5).[37]

With increasing Cu^{2+} concentration, the adsorption capacity rapidly increases, but the adsorption efficiency significantly decreases. At lower initial Cu^{2+} concentrations, the active sites on the adsorbent can quickly capture Cu ions from the solution until all Cu^{2+} ions are completely adsorbed. The adsorption isotherms of BC-CLS were studied at 298 K, and the Langmuir, Freundlich and Temkin models were applied to validate the adsorption data. As shown in Table 2, the fitting correlation of the Langmuir model is higher than that of the Freundlich model and Temkin model, indicating that the Langmuir model

Table 2 Isotherm parameters of the adsorbents for Cu^{2+}

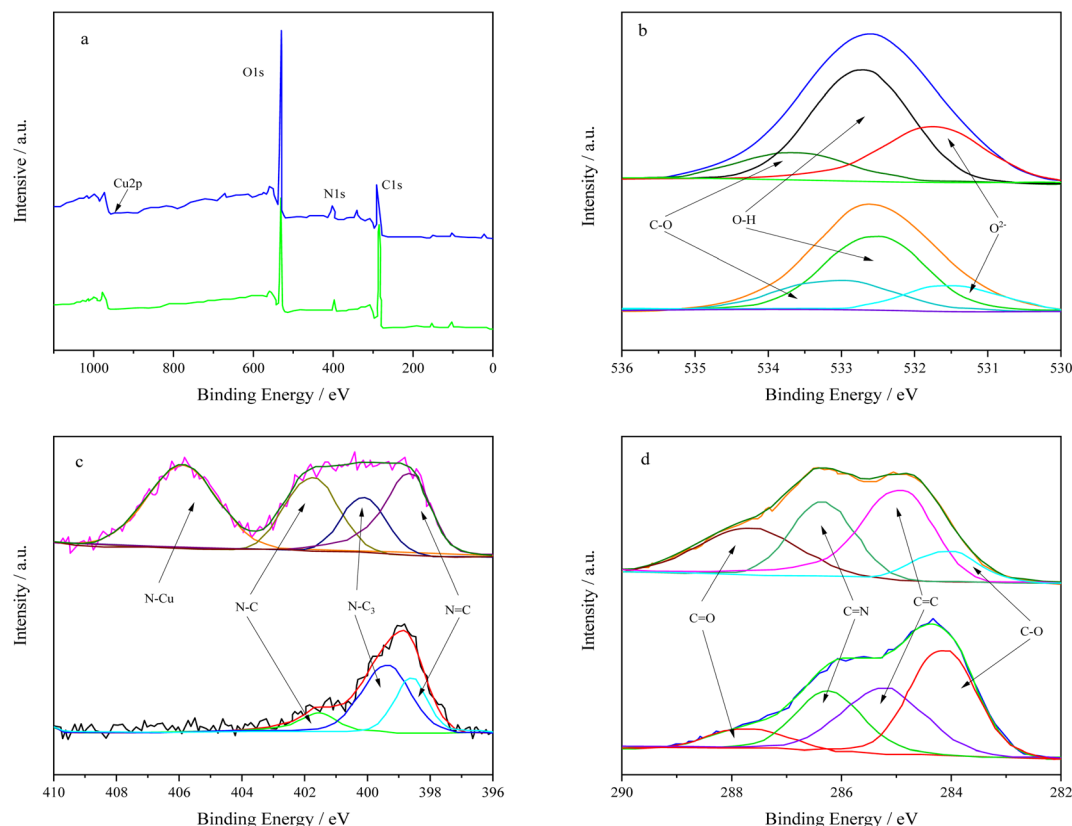| Adsorbate	Cu^{2+}
Langmuir	
q_m (mg g^{-1})	393.89
K_L (L mg^{-1})	0.141
R^2	0.9989
Freundlich	
K_F (L g^{-1})	436.64
$1/n$	0.0142
R^2	0.9897
Temkin	
A (mg L^{-1})	10.62
B	44.36
R^2	0.8969

Fig. 6 Complete XPS spectra of BC-CLS and BC-CLS-Cu (a), high resolution of O 1s (b), high resolution of N 1s (c), high resolution of C 1s (d) (experiment condition: adsorbent dose 0.01 g, temperature 298 K, pH 5, time 120 min, concentration 100 mg g^{-1}, solution volume 50 mL).
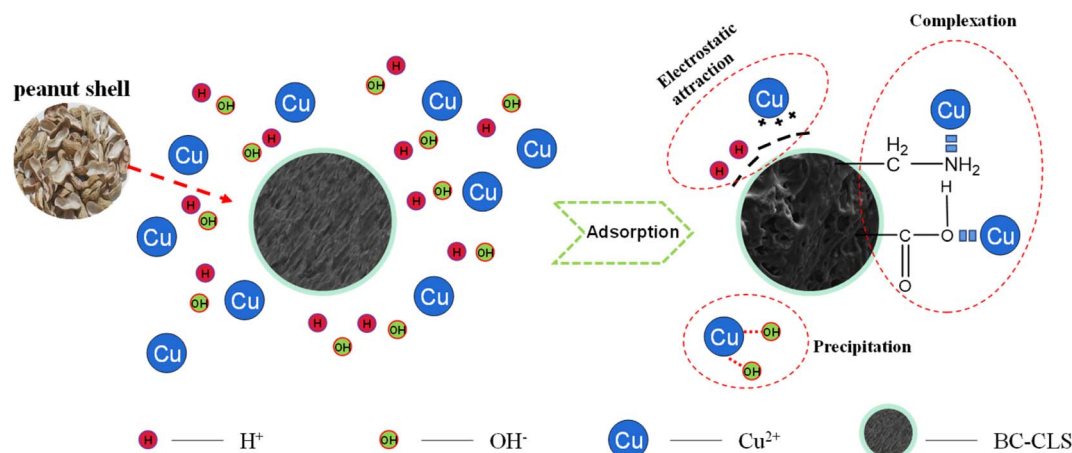

Fig. 7 Assumption of adsorption mechanism of BC-CLS.

is suitable for describing the removal behavior of BC-CLS for Cu^{2+}. These results suggest that the removal of Cu^{2+} by BC-CLS is controlled by uniform monolayer adsorption.

3.4 Adsorption mechanism

In order to further understand the interaction mechanism between BC-CLS and Cu^{2+}, the XPS spectra of BC-CLS and BC-CLS-Cu were further studied. As shown in Fig. 6a, new peaks were observed in the XPS spectrum of BC-CLS-Cu, which were

around 933.5 eV, indicating the presence of Cu 2p peaks and further confirming the adsorption of Cu on the surface of BC-CLS. As shown in Fig. 6b, the high-resolution XPS of O 1s can be divided into three peaks: O^{2-} oxide at 531.6 eV, –OH at 532.2 eV, and C–O at 533.4 eV. After adsorption, the peaks of O^{2-} oxide, O–H, and C–O shifted to higher binding energies, confirming the important active sites of oxygen-containing functional groups in coordinating Cu. From Fig. 6c, the peaks at 398.7, 399.1, and 402.0 eV can be attributed to C=N, N–C$_3$, and
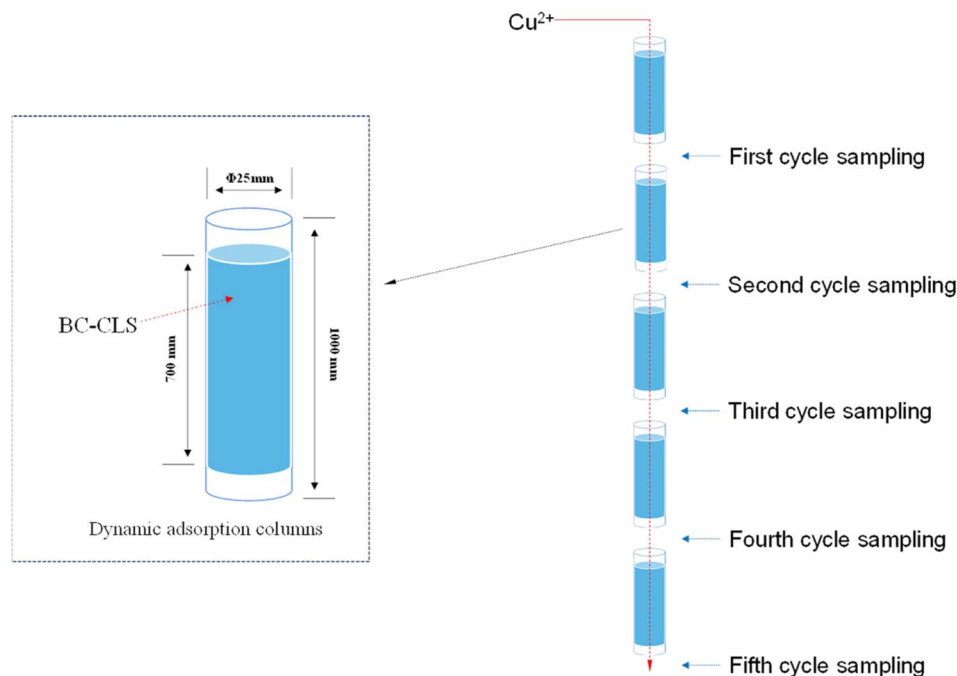
Fig. 8 Dynamic adsorption schematic (experiment condition: adsorbent dose 0.01 g, temperature 298 K, pH 5, time 120 min, concentration 100 mg g^{-1}, solution volume 50 mL).

C–N of BC-CLS, respectively. After adsorption, a new peak appeared at 406.2 eV, which may be related to the nitrogen formed after binding with Cu. As shown in Fig. 6d, the peaks at 284.4, 285.1, 286.3, and 287.5 eV can be attributed to C–O, C=C, C=N, and C=O of BC-CLS, respectively. After Cu adsorption, the content of C–O decreased significantly, further indicating the involvement of oxygen/nitrogen-containing functional groups in the adsorption process. In summary, the interaction between active functional groups and Cu complexes plays a dominant role in the capture of Cu ions during adsorption.

From the results of studying the effect of pH on adsorption, it is found that the protonation of BC-CLS affects the adsorption of

Cu, indicating the existence of electrostatic attraction between BC-CLS and Cu. As the pH increases, OH- in the solution will combine with Cu ions to form insoluble hydroxides, which will also Cu to a decrease in the concentration of Cu. In conclusion, the adsorption between BC-CLS and Cu is controlled by multiple mechanisms, including metal complexation, electrostatic attraction, and precipitation, as shown in Fig. 7.

3.5 Dynamic adsorption experiment

In practical applications, the adsorbent is in a dynamic environment, so it is important to study the dynamic adsorption capacity of BC-CLS. At pH = 4, the dynamic adsorption efficiency of 10 mg BC-CLS for Cu^{2+} at different initial concentrations (10, 20, 30 mg L^{-1}) was studied. At 10 mg L^{-1} Cu^{2+}, after one cycle of liquid circulation, 70% of Cu^{2+} was removed from the solution, and after 5 cycles, the residual Cu^{2+} in the solution was only about 0.4 mg L^{-1}, which already meets the national discharge standard for Cu^{2+} in wastewater (1 mg L^{-1}). BC-CLS can almost completely separate Cu^{2+} from water at low Cu^{2+} concentrations, further demonstrating its potential as a material for Cu^{2+} separation that can be applied on a large scale. In the case of 10 mg L^{-1} Cu^{2+}, after five cycles of liquid circulation, BC-CLS still achieved a removal efficiency of over 99% for Cu^{2+}. These results indicate that BC-CLS has excellent dynamic adsorption capacity and can be used as a promising adsorbent for removing Cu^{2+} from wastewater (Fig. 8).
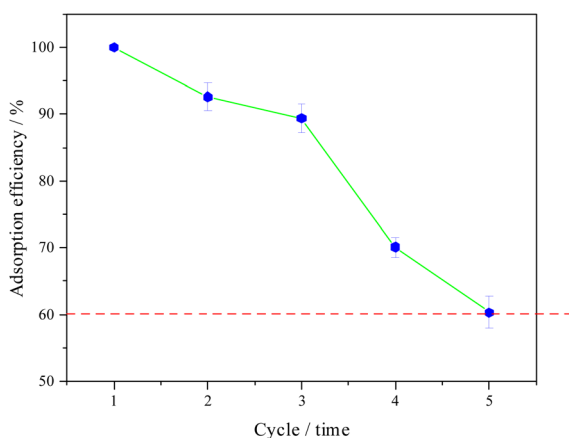

Fig. 9 Adsorption efficiency of BC-CLS after different adsorption–desorption (experiment condition: adsorbent dose 0.01 g, temperature 298 K, pH 5, time 120 min, concentration 100 mg g^{-1}, solution volume 50 mL).

3.6 Adsorption–desorption

From Fig. 3a, it can be seen that the adsorption capacity of BC-CLS decreases at higher H$^+$ concentrations. Additionally,

Table 3 Comparison of adsorption capacities of several adsorbents for Cu^{2+}

Adsorbent	Adsorbate	Maximum adsorption capacity (mg g^{-1})	References
CIP	Pb^{2+}	35.41	6
MBA-bead	Cu^{2+}	234.1	8
CS-BC	Methylene blue	499.8	11
Lignin-biochar	Pb^{2+}	679	12
LMB	Pb^{2+}	152.58	20
BC-CLS	Cu^{2+}	354	This work

lowering the pH value can promote the desorption of Cu^{2+} from BC-CLS. When using HCl solution as the eluent, Cu^{2+} can be easily desorbed from BC-CLS. Furthermore, from Fig. 9, it can be observed that the adsorption efficiency of BC-CLS decreases during the adsorption/desorption process. The reason for the decrease of adsorption performance may be that not all adsorbents are separated during the desorption process, and it can be known that the solubility of the solution after desorption is less than the adsorption capacity. However, BC-CLS still maintains 60% adsorption efficiency after 5 cycles, which demonstrates its good stability and ability to be reused multiple times.

The adsorption capacity of BC-CLS for Cu^{2+} was compared with other carbon adsorbents reported in the recent references. Although the maximum adsorption performance of BC-CLS is not the best among the listed results (Table 3), BC-CLS can still be used as an efficient adsorbent.

4 Conclusion

The BC-CLS adsorbent was obtained by using natural raw materials, peanut shell, and lignin composite. The SEM, BET and FT-IR analysis results showed that the combination of biochar and lignin caused changes in the chemical properties and physical structure of the material. BC-CLS has the characteristics of short adsorption time (50 min), fast adsorption rate (11 mg g^{-1} min^{-1}), and high static saturation adsorption capacity (354 mg g^{-1}), and it can effectively remove Cu^{2+} from water through dynamic cycling adsorption. The adsorption study showed that pH value had a significant impact on the adsorption of Cu^{2+} by BC-CLS. The pseudo-second-order kinetic model fit the adsorption experimental data, and the Langmuir isotherm model fit the adsorption equilibrium data. The adsorption mechanism indicated that the surface complexation was the main interaction between BC-CLS and Cu^{2+}, accompanied by electrostatic adsorption and precipitation. After 5 adsorption–desorption cycles, BC-CLS still exhibited good adsorption capacity, confirming its practical applicability.

Conflicts of interest

The authors declare that they have no known competing financial interests or personal relationships that could have appeared to influence the work reported in this paper.

Acknowledgements

References

1 Li, M. Guo, Y. Wang, H. Deng, L. Hou, C. Yu and Z. Liu, Selective adsorption of heavy metal ions by different composite-modified semi-carbonized fibers, *Sep. Purif. Technol.*, 2024, **328**, 125022.

2 B. Gao, J. Zhang, J. Liu, A. Ali and M. Sillanpää, Excess sludge-based biochar loaded with manganese enhances catalytic ozonation efficiency for landfill leachate treatment, *Environ. Pollut.*, 2024, **346**, 123591.

3 Gao, Q. Lin, T. Yang, Y. C. Bao and J. Liu, Preparation and characterization of ZSM-5 molecular sieve using coal gangue as a raw material via solvent-free method: Adsorption performance tests for heavy metal ions and methylene blue, *Chemosphere*, 2023, **341**, 139741.

4 Y. Man, D. Liu, S. Shang, Z. Song, Y. Qi, L. Huang and S. Cui, A novel magnetic Fe_3O_4/cellulose nanofiber/polyethyleneimine/thiol-modified montmorillonite aerogel for efficient removal of heavy metal ions: Adsorption behavior and mechanism study, *Int. J. Biol. Macromol.*, 2023, **253**(Part 3), 126634.

5 Sun, Z. Jiang, L. Chen and Y. Zhao, Preparation of CTS/PAMAM/SA/Ca^{2+} hydrogel and its adsorption performance for heavy metal ions, *Appl. Surf. Sci.*, 2023, **607**, 155135.

6 Li, T. Liu, H. Xing, Y. Li and X. Ma, Removal of heavy metals lead and ciprofloxacin from farm wastewater using peanut shell biochar, *Environ. Technol. Innovation*, 2023, **30**, 103121.

7 Ballu Duwiejuah, A. K. Quainoo and A.-H. Abubakari, Simultaneous adsorption of toxic metals in binary systems using peanut and sheanut shells biochars, *Heliyon*, 2022, **8**(9), e10558.

8 Salem, A. Ouakouak, F. Touahra, N. Hamdi, A. S. Eltaweil, A. Syed, R. Boopathy and H. N. Tran, Easy separable, floatable, and recyclable magnetic-biochar/alginate bead as super-adsorbent for adsorbing copper ions in water media, *Bioresour. Technol.*, 2023, **383**, 12922.

9 Li, W. Tian, M. Chu, M. Zou and J. Zhao, Molecular imprinting functionalization of magnetic biochar to adsorb sulfamethoxazole: Mechanism, regeneration and targeted adsorption, *Process Saf. Environ. Prot.*, 2023, **171**, 238–249.

10 Hopa, A. Eraghi Kazzaz and P. Fatehi, Fabrication of carboxyalkylated lignin derived microgels for adsorbing heavy metals, *Ind. Crops Prod.*, 2022, **187**(Part B), 115482.

11 Liu, M.-F. Li, J.-F. Ma, J. Bian and F. Peng, Chitosan crosslinked composite based on corncob lignin biochar to adsorb methylene blue: Kinetics, isotherm, and thermodynamics, *Colloids Surf., A*, 2022, **642**, 128621.

12 L. Yuan, F. Wang, Y. Miao, Y. Mai, H. Li, X. Chen and J. Chen, A lignin-biochar with high oxygen-containing groups for

adsorbing lead ion prepared by simultaneous oxidization and carbonization, *Bioresour. Technol.*, 2020, **307**, 123165.

13 Hopa, A. Eraghi Kazzaz and P. Fatehi, Fabrication of carboxyalkylated lignin derived microgels for adsorbing heavy metals, *Ind. Crops Prod.*, 2022, **187**(Part B), 115482.

14 Zhang, Y. Chen, D. Wang, D. Yu and C. Wu, Lignin-based adsorbents for heavy metals, *Ind. Crops Prod.*, 2023, **193**, 116119.

15 Zheng, F. Seidi, W. Wu, Y. Pan and H. Xiao, Dual-functional lignin-based hydrogels for sustained release of agrochemicals and heavy metal ion complexation, *Int. J. Biol. Macromol.*, 2023, **235**, 123701.

16 Lu, H. Xu, S. Wei, F. Jiang, J. Zhang, Y. Ge and Z. Li, In situ doping lignin-derived carbon quantum dots on magnetic hydrotalcite for enhanced degradation of Congo Red over a wide pH range and simultaneous removal of heavy metal ions, *Int. J. Biol. Macromol.*, 2023, **239**, 124303.

17 Justo Santos, J. Paggiaro, H. D. C. Silva Pimentel, A. Karla dos Santos Pereira, G. Soares Cavallini and D. H. Pereira, Computational study of the interaction of heavy metal ions, Cd(II), Hg(II), and Pb(II) on lignin matrices, *J. Mol. Graphics Modell.*, 2022, **111**, 108080.

18 Gong, H. Wu, X. Shan and Z. Li, Facile fabrication of phosphorylated alkali lignin microparticles for efficient adsorption of antibiotics and heavy metal ions in water, *J. Environ. Chem. Eng.*, 2021, **9**(6), 106574.

19 G. Fouda-Mbanga, E. Prabakaran and K. Pillay, Carbohydrate biopolymers, lignin based adsorbents for removal of heavy metals (Cd^{2+}, Pb^{2+}, Zn^{2+}) from wastewater, regeneration and reuse for spent adsorbents including latent fingerprint detection: A review, *Biotechnol. Rep.*, 2021, **30**, e00609.

20 Tan, Y. Zhang, W. Zhang, R. Zhao, R. Yue and T. Liu, One-pot method to prepare lignin-based magnetic biosorbents for bioadsorption of heavy metal ions, *Ind. Crops Prod.*, 2022, **176**, 114387.

21 A. Ali, B. Tanhaei, H. Beiki, P. Krivoshapkin, E. Krivoshapkina and C. Tracey, Insight into the adsorptive removal of ibuprofen using porous carbonaceous materials: A review, *Chemosphere*, 2023, **323**, 138241.

22 Yang, G. Ji, Y. Gao, W. Fu, M. Irfan, L. Mu, Y. Zhang and A. Li, High-yield and high-performance porous biochar produced from pyrolysis of peanut shell with low-dose ammonium polyphosphate for chloramphenicol adsorption, *J. Cleaner Prod.*, 2020, **264**, 121516.

23 An, N. Jin, S. Deng, B. Zhao, M. Liu, B. Ran and L. Zhang, Ni(II), Cr(VI), Cu(II) and nitrate removal by the co-system of Pseudomonas hibiscicola strain L1 immobilized on peanut shell biochar, *Sci. Total Environ.*, 2022, **814**, 152635.

24 X. Chao, X. Qian, Z. Han-hua, W. Shuai, Z. Qi-hong, H. Dao-you and Z. Yang-zhu, Effect of biochar from peanut shell on speciation and availability of lead and zinc in an acidic paddy soil, *Ecotoxicol. Environ. Saf.*, 2018, **164**, 554–561.

25 Wu, J. Ming, W. Zhou, N. Xiao and J. Cai, Efficiency and mechanism in preparation and heavy metal cation/anion adsorption of amphoteric adsorbents modified from various plant straws, *Sci. Total Environ.*, 2023, **884**, 163887.

26 L. Popovic, J. D. Rusmirovic, Z. Velickovic, T. Kovacevic, A. Jovanovic, I. Cvijetic and A. D. Marinkovic, Kinetics and column adsorption study of diclofenac and heavy-metal ions removal by amino-functionalized lignin microspheres, *J. Ind. Eng. Chem.*, 2021, **93**, 302–314.

27 Chen, S. I. S. Shahabadi, D. Zhou, W. Liu, J. Kong, J. Xu and X. Lu, Facile preparation of cross-linked lignin for efficient adsorption of dyes and heavy metal ions, *React. Funct. Polym.*, 2019, **143**, 104336.

28 Xiao, W. Ding, J. Zhang, Y. Ge, Z. Wu and Z. Li, Fabrication of a versatile lignin-based nano-trap for heavy metal ion capture and bacterial inhibition, *Chem. Eng. J.*, 2019, **358**, 310–320.

29 L. Popovic, J. D. Rusmirovic, Z. Velickovic, Z. Radovanovic, M. Ristic, V. P. Pavlovic and A. D. Marinkovic, Novel amino-functionalized lignin microspheres: High performance biosorbent with enhanced capacity for heavy metal ion removal, *Int. J. Biol. Macromol.*, 2020, **156**, 1160–1173.

30 Wang, C. Jiang, B. Hou, Y. Wang, H. Chen and J. Wu, Carbon composite lignin-based adsorbents for the adsorption of dyes, *Chemosphere*, 2018, **206**, 587–596.

31 Guo, Z. Zou, Y. Chen, X. Long, M. Liu, X. Li, J. Tan and R. Chen, Synergistic effect of hydrogen bonding and π-π interaction for enhanced adsorption of rhodamine B from water using corn straw biochar, *Environ. Pollut.*, 2023, **320**, 121060.

32 Z. Wang, A. Alinezhad, R. Sun, F. Xiao and J. J. Pignatello, Pre- and Postapplication Thermal Treatment Strategies for Sorption Enhancement and Reactivation of Biochars for Removal of Per- and Polyfluoroalkyl Substances from Water, *ACS ES&T Eng.*, 2023, **3**(2), 193–200.

33 Yang, X. Sun, Q. Li, C. Lin, R. Wang, X. Sun, L. An, W. Chen, L. Wei and Q. An, Fabrication of multifunction-integrated adsorbent based on zwitterion functionalized cellulose with high adsorption performance for anionic/cationic dyes and heavy metal ions, *Colloids Surf., A*, 2024, **683**, 133012.

34 Shye Chong, M. A. Manan and A. Kamal Idris, Sodium lignosulfonate as sacrificial agent and effectiveness in reducing CTAB cationic adsorption onto kaolinite, *J. King Saud Univ., Eng. Sci.*, 2021, **33**(8), 539–546.

35 Wang, J. Wang, L. Jiang and Y. Jiang, Adsorption of Pb^{2+} and Cu^{2+} in wastewater by lignosulfonate adsorbent prepared from corn straw, *Int. J. Biol. Macromol.*, 2023, **247**, 125820.

36 Chen, W. Zhang, Y. Ye, X. Ying, J. Huang and X. Li, Introduction of aminated sodium lignosulfonate as a chain extender for preparation of high-performance waterborne polyurethane, *Int. J. Adhes. Adhes.*, 2023, **125**, 103415.

37 Jiang, X. Wang, X. Wang, B. Hou, H. Chen, X. Li and J. Wu, Construction of a Lignosulfonate–Lysine Hydrogel for the Adsorption of Heavy Metal Ions, *J. Agric. Food Chem.*, 2020, **68**(10), 3050–3060.